Optical and atomic stochastic resonances in the driven dissipative Jaynes-Cummings model

Qingyang Qiu, Shengdan Tao, Cunjin Liu, Shengguo Guan, Min Xie, and Bixuan Fan*
College of Physics and Communication Electronics, Jiangxi Normal University, Nanchang 330022, China
(Received 21 July 2017; published 6 December 2017)

In this paper, we study the stochastic resonance (SR) effect in a driven dissipative Jaynes-Cummings model. The SR effect is systematically investigated in the semiclassical and full quantum frameworks, and in both cases we find that SRs simultaneously occur for optical and atomic degrees of freedom. In particular, at zero temperature, quantum SR can be induced merely by vacuum fluctuations. Although the qualitative features of semiclassical SR and quantum SR are similar, their mechanisms are completely different: semiclassical SR is induced by thermal activation while quantum SR is induced by quantum-tunneling-assisted transitions. Our results provide a theoretical basis for experimentally observing and studying the SR phenomenon of the Jaynes-Cummings model in the quantum regime.

DOI: 10.1103/PhysRevA.96.063808

I. INTRODUCTION

Stochastic resonance (SR) [1–4] is a phenomenon in which a suitable level of noise in a nonlinear system can induce coherent amplification of the system response to an external weak signal. A typical SR example is a bistable model subject to a subthreshold periodic signal and a noisy environment. When the time scales of the noise and the signal satisfy a certain matching condition, the system dynamics can be switched from small-amplitude intrawell oscillations to large-amplitude interwell oscillations, resulting in significant signal amplification. In the classical world, SR has been extensively studied in a variety of research fields [3,4] and has been widely applied in weak signal detection [5,6] and amplification [7–9].

Recently, increasing interest has been directed toward studying SR in the quantum domain, such as in the quantum nonlinear oscillator system [10], the maser system [11], the Dicke model [12], the spin-boson model [13], the quantum many-body system [14], the four-level atomic system [15], and the cavity optomechanical system [16]. However, most work on quantum SR has been at low but nonzero temperature, where thermal noise and quantum noise coexist. Work on SR induced by purely quantum fluctuations at zero temperature has been very rare [10,17]. The investigation of the interplay between purely quantum fluctuations and nonlinearity in the context of SR may help to further understand the quantum nature of the SR effect.

In this paper, we aim to study the SR phenomenon induced by quantum fluctuations in the Jaynes-Cummings (JC) model [18,19] at zero temperature. The JC model is one of most important and fundamental models in quantum optics, and this model and its generalizations describe many of the interactions between fields and natural atoms [20] or artificial matter (such as the superconducting circuit system [21] and the quantum dot system [22]). Therefore, theoretical study of SR in the JC model has great potential to be realized in various practical quantum systems.

Through systematic study of the SR phenomenon in the JC model in both the semiclassical and full quantum frames, we find that in both cases the optical and atomic modes can exhibit SR behavior. In particular, in the full quantum description we use the quantum trajectory theory [23] to mimic the system stochastic dynamics conditioned on noisy homodyne detection records. We show that, at zero temperature, vacuum fluctuations can induce periodic quantum switching between two metastable states with the same period as that of the input weak signal, which is known as the synchronization effect in SR. Quantum SR is qualitatively similar to SR in the semiclassical framework, but their noise sources, required parameter regimes, and optimal signal frequencies are different. Moreover, we present an approach for searching for conditions that favor SR in a general nonlinear system. The system parameters we use are feasible for current experiment conditions, i.e., the single-Cs-atom QED system [20] and the superconducting circuit system [21]. Therefore, our analysis lays the theoretical basis for experimental observation of SR phenomena in the JC model. Furthermore, there are potential applications in quantum signal detection based on the SR mechanism in this fundamental quantum optics model.

The paper is organized as follows. In Sec. II, we introduce the model, find the bistability region for the cavity field and the atom, and present noise-activated stochastic bistable transitions. In Sec. III, we show the SR features with their semiclassical description, including residence time distributions, synchronization between the input signal and the system responses, and the resonancelike effect of the signal-to-noise ratio (R_{SN}) curve. In Sec. IV, the SR effect in the full quantum-mechanical framework is studied and the differences between quantum and semiclassical SR are discussed. Finally, we conclude our paper in Sec. V.

II. MODEL AND EQUATIONS

As shown in Fig. 1, the system considered is a two-level atom (a qubit) interacting with a single-mode cavity field, that is, the well-known JC model. The cavity is driven by two fields: one strong control field E_1 with frequency ω_{d1} and one weak signal field E_2 with frequency ω_{d2}. We assume that the driving field E_1 is exactly resonant with the atomic transition frequency and the cavity central frequency. In the rotating frame at the driving frequency ω_{d1}, the Hamiltonian for the

*bixuanfan@jxnu.edu.cn

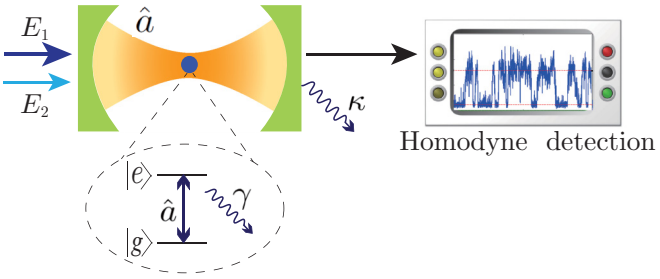

FIG. 1. Schematic: A two-level atom (a qubit) interacts with a single-mode cavity field and with two driving fields E_1 and E_2. E_1 is a strong control field resonant with the cavity mode and E_2 is a weak signal field slightly detuned from the cavity mode. The output of the cavity is detected by homodyne detection.

described system is given by ($\hbar = 1$)

$$\hat{H}_s = g(\hat{\sigma}_+\hat{a} + \hat{a}^\dagger\hat{\sigma}_-) - iE_1(\hat{a} - \hat{a}^\dagger) - iE_2(\hat{a}e^{i\delta t} - \hat{a}^\dagger e^{-i\delta t}) \tag{1}$$

where $\delta = \omega_{d2} - \omega_{d1}$. g is the atom-field interaction coefficient, $\hat{a}$ ($\hat{a}^\dagger$) is the annihilation (creation) operator for the cavity field, and $\hat{\sigma}_- = |g\rangle\langle e|$ [$\hat{\sigma}_+ = (\hat{\sigma}_-)^\dagger$] is the atomic lowering [raising] operator.

To investigate the SR effect in our system, the first step is to find a bistable region and prepare a threshold for SR occurrence. We first search for the steady-state solutions and study system stability properties in the semiclassical description. By neglecting quantum fluctuations of the field and the atom, we write the classical Langevin equations by replacing quantum operators with classical complex variables $\hat{a} \to \alpha$, $\hat{\sigma}_- \to p$, and $\hat{\sigma}_z \to D_0$:

$$\dot{\alpha} = -\frac{\kappa}{2}\alpha - igp + E_1 + E_2 e^{-i\delta t} + \xi, \tag{2}$$

$$\dot{p} = -\frac{\gamma}{2}p + ig\alpha D_0, \tag{3}$$

$$\dot{D}_0 = -\gamma(D_0 + 1) - 2ig(\alpha p^* - \alpha^* p) \tag{4}$$

where we have phenomenologically introduced the cavity decay rate κ and the atomic relaxation rate γ. The stochastic thermal noise ξ satisfies $\langle\xi(t)\xi(t')\rangle = 2D\delta(t - t')$ with D being the noise strength. In the absence of the weak signal $E_2 e^{-i\delta t}$, we have the steady-state results for the optical-field amplitude α and the atomic population inversion D_0 by setting time derivatives in Eqs. (2)–(4) to zeros:

$$E_1 = \frac{\kappa\alpha}{2}\left(\frac{2C}{1 + |\alpha|^2/n_0} + 1\right), \tag{5}$$

$$4E_1^2 D_0 = n_0\kappa^2(1 - D_0)(1 + 2CD_0)^2 \tag{6}$$

where we have defined the cooperation coefficient as $C = 2g^2/(\kappa\gamma)$ and the saturation photon number as $n_0 = \gamma^2/(8g^2)$.

Under the resonance condition, α is real and Eqs. (5) and (6) are cubic equations for α and D_0, which in principle have three roots in suitable parameter regimes. Equation (5) reproduces the familiar expressions for optical absorptive bistability in the JC model [24], and bistability appears for the cooperation coefficient $C > 4$. Here we choose $C = 6$ and in Fig. 2 we plot the bistability curves for the optical-field

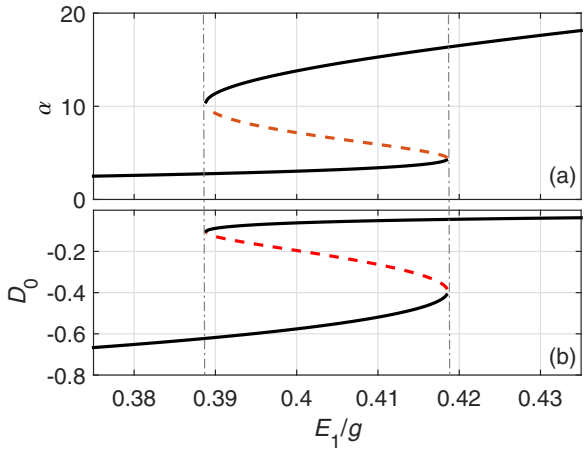

FIG. 2. Simultaneous bistability in the optical (a) and atomic (b) degrees of freedom. The stable and unstable solutions are denoted by the solid black curves and the dashed red curves, respectively. The parameters are $g = 1$, $\kappa = g/30$, $\gamma = 10g$, and $E_2 = 0$.

amplitude α and atomic population inversion D_0. It is evident that optical and atomic bistabilities share exactly the same region (labeled by the gray dash-dotted lines), in which α and D_0 have three solutions (two stable and one unstable solutions). The stability properties were determined by the standard linear analysis method [25]. Under this parameter setting, the saturation photon number ($n_0 = 12.5$) is far greater than unity, indicating that the system operates beyond the quantum regime. Therefore, quantum fluctuations can be neglected safely and the semiclassical approximation is well satisfied.

We then include the noise ξ and study the stochastic dynamics in the absence of the weak signal. By choosing a driving amplitude in the middle of the bistable region ($E_1 = 0.398g$), we numerically show the random transitions of the system dynamics between two metastable states activated by the thermal noise $D = 0.025$ [Fig. 3(a)]. Clear, sharp transitions between two states can be seen in both optical and atomic modes, and the transitions are exactly simultaneous. The corresponding distributions of two metastable states of the field are shown in Fig. 3(b), and they exhibit the expected bimodal structure. The distribution of the low-amplitude state (L) features a narrow, high peak while the distribution of the high-amplitude state (H) features a wider, lower peak. These behaviors can be verified from the potential function. The effective position variable for the cavity field can be defined as $x = (\alpha + \alpha^*)/2 = \alpha$. Under the condition of $\gamma \gg \kappa, g$, one can adiabatically eliminate the atomic variables and obtain the approximate equation for the optical mode alone as

$$\ddot{\alpha} + \frac{\kappa + \gamma}{2}\dot{\alpha} \approx \frac{\gamma}{2}E_1 - \frac{\kappa\gamma}{4}\alpha - \frac{g^2\alpha}{1 + 8g^2|\alpha|^2/\gamma^2}. \tag{7}$$

The approximate effective potential function can then be obtained by integrating the right-side expression of Eq. (7) over α:

$$U(\alpha) \approx \frac{\kappa\gamma}{8}\alpha^2 - \frac{\gamma E_1}{2}\alpha + \frac{\gamma^2}{16}\ln(1 + 8g^2\alpha^2/\gamma^2). \tag{8}$$

In Fig. 3(c), we plot the potential function of the optical field $U(\alpha)$ using the same parameters as shown in Fig. 3(a). There

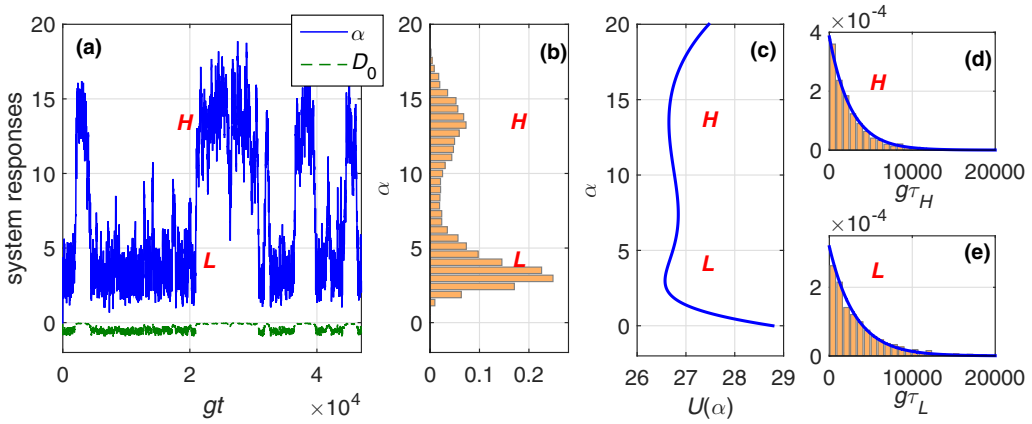

FIG. 3. (a) Simultaneous stochastic transitions of the optical-field amplitude α and the atomic population inversion D_0 in the absence of the signal E_2. H and L denote the high- and low-amplitude states of the optical field, respectively. (b) Histogram of α using the data (the solid blue curve) in panel (a). (c) Effective potential function $U(\alpha)$ as a function of α calculated from Eq. (8). (d, e) Residence time (τ_j, $j = H,L$) distributions of the high- and low-amplitude states of the field for a long evolution time ($T = 1\,000\,000 g^{-1}$), respectively. The blue curves show the exponential fit $[1/\bar{\tau}_j \exp(-1/\bar{\tau}_j)]$ (j = H,L) to the data, with $\bar{\tau}_H = 2600 g^{-1}$ and $\bar{\tau}_L = 3140 g^{-1}$ for the higher-amplitude state (d) and the lower-amplitude state (e), respectively. The parameters are $g = 1$, $\kappa = g/30$, $\gamma = 10g$, $E_1 = 0.398g$, and $D = 0.025$.

are two asymmetric wells in the potential function: a wide well at high amplitude and a narrow well at low amplitude. This is consistent with the distribution in Fig. 3(b). From Figs. 3(a)–3(c), one may note that there is a correlation between the widths of the potential wells and the variances of the amplitude fluctuations. The wider the potential well, the larger the variance of the dynamics for the corresponding metastable state.

Figures 3(d) and 3(e) show the residence time distributions, that is, the distributions of time intervals of the system dwelling in the high-amplitude state [Fig. 3(d)] or the low-amplitude state [Fig. 3(e)]. In order to estimate the average residence time, we use the exponential decay function $1/\bar{\tau}\exp(-1/\bar{\tau})$ to fit the data in Figs. 3(d) and 3(e); the fitting results are $\bar{\tau_H} = 1/2600 g^{-1}$ and $\bar{\tau_L} = 1/3100 g^{-1}$. The difference in the average resident times of the high- and low-amplitude states results from the asymmetry of potential wells.

III. SR PHENOMENA IN THE SEMICLASSICAL FRAME

In the previous section, we found the bistable region and studied the thermal-noise-activated random transitions between two metastable states of the system in the absence of the weak modulation signal $E_2 e^{-i\delta t}$. In this section we add this signal to the system and study the SR phenomena using the semiclassical description [Eqs. (2)–(4)].

Before simulating the system dynamics, we need to fix two signal parameters in order to observe SR: a subthreshold amplitude E_2 and a suitable modulation frequency δ. The first is easy to determine by switching off the noise ($D = 0$): if the system experiences interwell transitions with this signal, then the signal exceeds the threshold; otherwise, the signal is below the threshold. Here we choose an amplitude slightly below the threshold, that is, $E_2 = 0.02g$. To determine a suitable modulation frequency δ, we recall the average

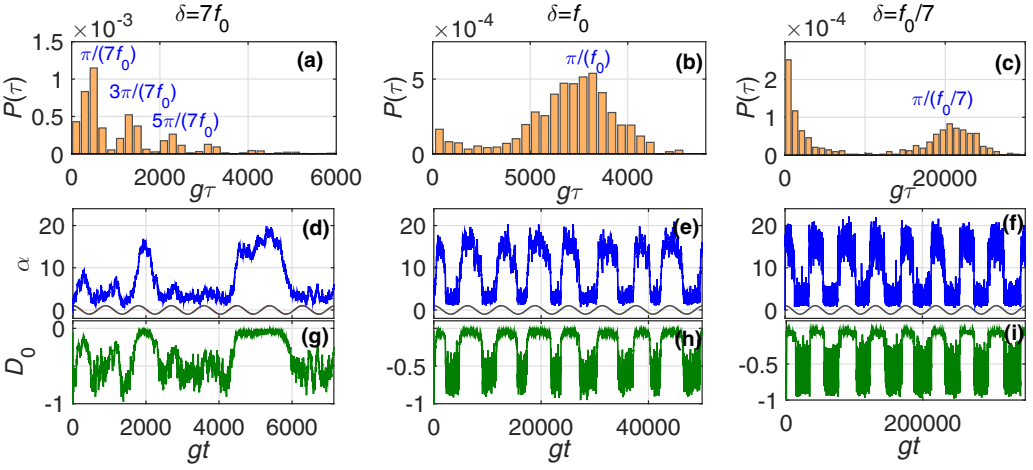

FIG. 4. Residence time distributions (a–c), optical responses (d–f), and atomic responses (g–i) for a system subjected to a weak signal and the noise for three values of modulation frequency δ in the semiclassical description: $\delta = 7f_0$ (a, d, g), $\delta = f_0$ (b, e, h), and $\delta = f_0/7$ (c, f, i). The parameters are $E_2 = 0.02g$ and $f_0 = 0.001g$, and other system parameters are the same as in Fig. 3.

transition time $\bar{\tau}$ obtained in the last section. The matching condition for SR is that the average transition time of the noise-induced random transitions is equal to half of the period of the external signal [3,26], that is, $\bar{\tau} = T_{E2}/2$. Then we can compute the optimal frequency under these parameters as $f_0 = 2\pi/T_{E2} = \pi/\bar{\tau}_L \approx 0.001g$. Note that if we choose $\bar{\tau}_H$ the optimal frequency is $f_0 \approx 0.0012g$, which makes no significant difference. Therefore, below, we use $f_0 = 0.001g$ as the optimal modulation frequency for simulating SR effect in the semiclassical regime.

In Fig. 4, we plot the residence time distributions of the high-amplitude state of the field (top row) and single trajectories of system responses (α in the middle row and D_0 in the bottom row) in the presence of a subthreshold weak signal $E_2 e^{-i\delta t}$ for three modulation frequencies ($7f_0$, f_0, and $f_0/7$). For the left column, the modulation frequency is much higher than the optimal frequency ($\delta = 7f_0$). If we consider only the system responses (α and D_0), the dynamics appear to be random, similar to spontaneous transitions in the case of no signal. However, the residence time distribution shows its correlation with the input signal and its distinguishing difference from noise-activated spontaneous transitions: several peaks separated by almost constant distance are located consistently according to the relation $\tau = (2n+1)T_{E2}/2$ with $n = 0,1,2\ldots$ [3,26].

The typical trajectories of system responses to the signal at the optimal frequency ($\delta = f_0$) are presented in the middle column. The system dynamics (blue and green curves) are synchronized with the input signal (gray curve). Correspondingly, the peak at half the periodicity of the signal occupies the majority of the residence time distribution, signaling the occurrence of the SR effect.

For the case of modulation frequency much lower than the optimal value ($\delta = f_0/7$), as shown in the right column, the periodicity in the system responses remains good but the system dynamics become noisier. There are two peaks in the residence time distribution: one exponentially decaying peak for noise-activated random transitions following Kramers's law [27] and the other peak for the signal, which is located at half the signal period. Compared to the optimal case (middle column), the proportion of the signal peak occupies much less area. Therefore, we have confirmed that only matched signal frequency and noise can result in the best SR effect.

We then present another feature of SR: a single resonancelike peak on the R_{SN} curve. The R_{SN} is defined as the height of the signal peak (P_s) relative to the background noise level (P_n) in the power spectrum of the output field $\sqrt{\kappa}\langle\hat{a}\rangle$ in units of dB; that is, $R_{SN}(\mathrm{dB}) = 10\log_{10}(R_{SN}) = 10\log_{10}(P_s) - 10\log_{10}(P_n)$. In Fig. 5, we plot the R_{SN} (dB) as a function of the thermal noise strength D on a logarithmic scale. As expected, the R_{SN} first increases and then decreases as the noise D increases, and the R_{SN} peaks over a wide range from 0.0002 to 0.7. A logarithmic scale is used for the x axis because the R_{SN} rises rapidly in the low-noise range and drops very slowly in the high-noise range.

In fact, the optimal values of D and δ in Fig. 4 for achieving the best SR effect for fixed system parameters (κ, γ, and g) are not unique. According to Kramers's rate $r_k \propto \exp(-\Delta V/D)$, the average transition rate of random transitions increases as the noise strength D increases, and the signal frequency required for satisfying the matching condition is larger. Therefore, increasing either D or δ requires the other to increase correspondingly in order to achieve the best SR effect.

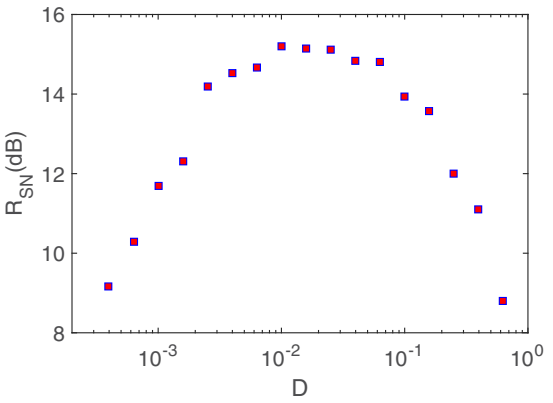

FIG. 5. The R_{SN} (dB) as a function of the thermal noise strength D at the modulation frequency $\delta = f_0 = 0.001g$. Every point is averaged over ten instances. The other parameters are the same as in Fig. 4.

IV. STOCHASTIC RESONANCE IN THE FULL QUANTUM FRAMEWORK

In the preceding sections, we studied stochastic bistable dynamics and the SR phenomenon in the semiclassical framework. In that case, to safely neglect quantum fluctuations and obtain the semiclassical equations, the system parameters are chosen to be beyond the quantum regime, i.e., $n_0 \gg 1$. Now we turn to the search for conditions leading to SR in the quantum regime and explore whether pure quantum fluctuations can induce the SR effect. In order to satisfy the high nonlinearity and quantumness of the system, we replace old parameters with a new set of parameters with large cooperativity C and low saturation photon number n_0, i.e, $C = 7.2$ and $n_0 = 0.3472$. For $n_0 < 1$, few photons or even a single photon inside the cavity can induce nonlinear system response, and quantum fluctuations play a significant role in the system.

To mimic reality in the model by including quantum noise and the signal detection process, in the quantum regime we study the system dynamics using the quantum trajectory method [23]. For a single trajectory or a single realization, the system dynamics conditioned on homodyne detection can be described by the stochastic master equation (SME) ($\hbar = 1$):

$$d\rho_I(t) = dt\{\, i[\rho_I(t), \hat{H}] + \mathcal{D}[\sqrt{\kappa}\hat{a}]\rho_I(t) + \mathcal{D}[\sqrt{\gamma}\hat{\sigma}_-]\rho_I(t)\} + dW(t)\mathcal{H}[\sqrt{\kappa}\hat{a}]\rho_I(t) \tag{9}$$

where $\hat{H}$ was given in Eq. (1) and dW is the Wiener increment [28] satisfying $\langle dW\rangle = 0$ and $\langle dW(t)^2\rangle = dt$. The superoperators $\mathcal{D}$ and $\mathcal{H}$ are defined as

$$\mathcal{D}[\hat{A}]\rho = \tfrac{1}{2}(2\hat{A}\rho\hat{A}^\dagger - \hat{A}^\dagger\hat{A}\rho - \rho\hat{A}^\dagger\hat{A}), \tag{10}$$

$$\mathcal{H}[\hat{A}]\rho = \hat{A}\rho + \rho\hat{A}^\dagger - \mathrm{Tr}[\hat{A}\rho + \rho\hat{A}^\dagger]\rho. \tag{11}$$

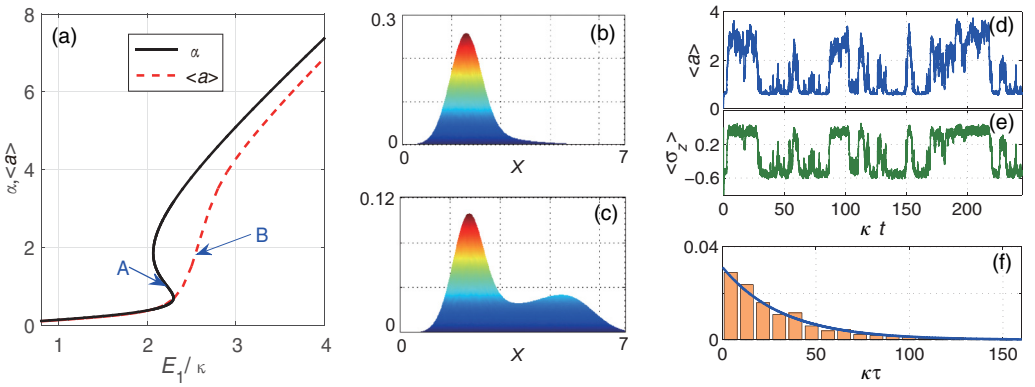

FIG. 6. (a) The semiclassical solution (α) and the quantum solution ($\langle\hat{a}\rangle$) for the amplitude of the cavity field at steady state. The parameters are $\kappa = 1$, $g = 6\kappa$, and $\gamma = 10\kappa$. (b, c) Wigner function distributions of the optical mode corresponding to points A and B in panel (a). (d, e) Typical trajectories for the optical-field amplitude $\langle\hat{a}\rangle$ and the atomic population inversion $\langle\hat{\sigma}_z\rangle$, respectively, obtained from the SME [Eq. (9)]. (f) Residence time distribution of the high-amplitude state of the field from long-time evolution ($T = 50\,000\kappa^{-1}$). The exponential fit function is $1/32\exp(-\tau/32)$.

The corresponding homodyne detection record is given by

$$I(t) = \sqrt{\kappa}\langle\hat{a} + \hat{a}^{\dagger}\rangle + dW(t)/dt. \tag{12}$$

By averaging the stochastic master equation [Eq. (9)] over all trajectories, we arrive at the unconditional master equation:

$$\dot{\rho(t)} = i[\rho(t), \hat{H}] + \mathcal{D}[\sqrt{\kappa}\hat{a}]\rho(t) + \mathcal{D}[\sqrt{\gamma}\hat{\sigma}_{-}]\rho(t) \tag{13}$$

where $\rho(t)$ is the ensemble average of the conditional density matrix $\rho_I(t)$ in the SME [Eq. (9)], that is, $\rho(t) = \mathcal{E}[\rho_I(t)]$. Through this unconditional master equation, we can obtain the averaged steady-state information of the system [see the dashed red curve in Fig. 6(a)]. To verify that this regime is quantum and the semiclassical approximation is invalid, we compare this quantum unconditional result with the semiclassical result [solid black curve in Fig. 6(a)] using the theory in Sec. II. We can see that the semiclassical bistable region does not overlap with the sharp transition region of the quantum curve. Unlike the classical bistable curve, the quantum curve has no hysteresis, as the bistable feature vanishes after averaging over all possible trajectories. In each trajectory—calculated from the SME [Eq. (9)]—as seen in Figs. 6(d) and 6(e), the bistable feature in the quantum case is manifested in switches between two metastable states. After averaging, there is only a sharply increasing region in the quantum curve shown in Fig. 6(a), and this region is not located in the middle of the classical bistability region; instead, it shifts to the larger driving side. The difference between the two curves is due to the invalidity of the factorization used in obtaining the semiclassical Langevin equations [Eqs. (2)–(4)] in the quantum regime. To confirm this, in Figs. 6(b) and 6(c), we plot the Wigner function distributions at two different driving strengths $E_1 = 2.25\kappa$ [labeled by point A in Fig. 6(a)] and $E_1 = 2.55\kappa$ [labeled by point B in Fig. 6(a)]. For $E_1 = 2.25\kappa$, the system is in the region of semiclassical bistability. However, as shown in Fig. 6(b), there is only a single peak in the phase space, which means that at this driving condition the system is actually monostable. For $E_1 = 2.55\kappa$, the system operates roughly at the middle point of the quantum curve in Fig. 6(a), while it is almost in the high-amplitude state in terms of the semiclassical solution. At this driving strength, the Wigner function distribution exhibits a double-peak structure. Based on these results it is clear that, with the new parameters (see the caption to Fig. 6), the system is in the quantum bistable regime and the semiclassical description is invalid.

Note that, in order to highlight the effect of pure quantum noise rather than thermal-noise-induced SR, here we consider the reservoir at zero temperature and study whether stochastic transitions can be induced by purely quantum fluctuations. We choose a driving scenario with $E_1 = 2.55\kappa$, in which the Wigner distribution is bimodal, and we plot the conditional dynamics of the system in Figs. 6(d) and 6(e). Clear quantum jumps are seen in the dynamics, and the jumps in optical and atomic modes are exactly simultaneous. Similar results can be found in Ref. [29]. Compared to the semiclassical results, quantum bistable dynamics have more small spikes and the transitions are less sharp.

To observe SR, we add the signal field $E_2 e^{-i\delta t}$ to the system. Again, we need to choose a suitable subthreshold amplitude and a suitable frequency for the signal. In the quantum case, we cannot judge the overthreshold or subthreshold signal from interwell transitions or intrawell transitions in the absence of quantum noise. When noise is absent, the system dynamics as described by the unconditional master equation [Eq. (13)] are an ensemble average of the conditional dynamics, and at every time the values of system variables are average values between two metastable states. In this situation, we can judge an overthreshold signal from whether the system dynamics are synchronized to the signal for an arbitrary frequency. A subthreshold signal can only induce good periodic system responses at a suitable frequency, and the synchronization is destroyed, especially at frequencies larger than the optimal value. The optimal frequency can be determined using the same procedure as in the semiclassical case: obtaining the average transition time from the residence time distribution of noise-induced spontaneous transitions and then calculating the optimal modulation frequency using the SR matching condition. We have shown the distributions of the residence time in the

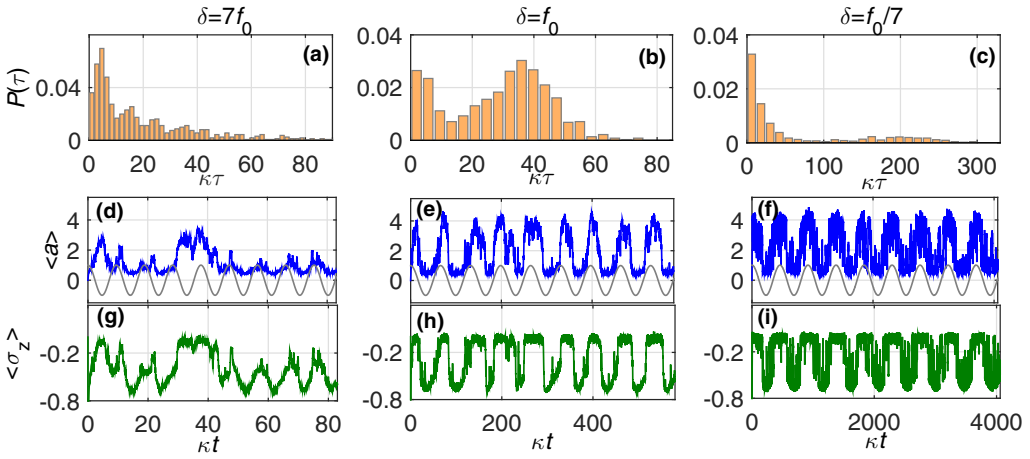

FIG. 7. Vacuum-fluctuation-induced SR. (a–c) Probability distributions of the residence time in the high-amplitude state of the field. (d–f) Responses of the optical mode to the vacuum noise and signal. (g–i) Responses of the atomic mode to the vacuum noise and signal. The signal modulation frequencies for the left, middle, and right columns are $7f_0$, f_0, and $f_0/7$ ($f_0 = 0.095\kappa$), respectively. The parameters are the same as in Fig. 6 except for $E_2 = 0.3\kappa$.

high-amplitude state of the field in Fig. 6(f), and from the fitting data we obtain the average transition time $\bar{\tau} \approx 32\kappa^{-1}$. We then obtain the approximate optimal signal modulation frequency $f_0 = 0.095\kappa$.

In Fig. 7, we show representative trajectories of system responses ($\langle\hat{a}\rangle$ and $\langle\hat{\sigma}_z\rangle$) and the corresponding residence time distributions subject to the input signal $E_2 e^{-i\delta t}$ for three values of the modulation frequency $\delta = 7f_0, f_0$, and $f_0/7$. SR behavior in the quantum picture is qualitatively similar to the situation in the semiclassical picture: system responses are synchronized to the signal best at an optimal modulation frequency f_0; a larger frequency $7f_0$ leads to poor periodicity, and a smaller frequency $f_0/7$ leads to noisier dynamics. However, there are several differences. First, their noise sources are different. Quantum SR is induced by quantum noise while semiclassical SR is activated by thermal noise. Second, the required parameters are different. Semiclassical SR works in the regime with large cooperativity and large saturation photon number, while quantum SR works in the regime with large cooperativity but small saturation photon number. Third, their optimal modulation frequencies are different, because different noise levels and different system parameters require different time scale or frequency scale of the signal to satisfy the SR matching condition.

V. CONCLUSION

We have studied stochastic resonance phenomena in the driven dissipative Jaynes-Cummings model in both semiclassical and full quantum frameworks. Simultaneous occurrence of SRs in the optical and atomic degrees of freedom have been numerically observed. In particular, at zero temperature, vacuum fluctuations can drive spontaneous bistable transitions and the SR effect, in which the input signal is amplified significantly. By comparing quantum SR with semiclassical SR, we found that they are qualitatively similar. However, they are driven by different noise sources: quantum SR is induced by quantum noise assisted tunneling while semiclassical SR is induced by thermal activation. Our results lay a theoretical basis for experimentally investigating SR in the JC model and its generalizations.

ACKNOWLEDGMENTS

The authors would like to thank Dr. Zhenglu Duan for helpful discussions. We gratefully acknowledge financial support from the National Natural Science Foundation of China under Grants No. 11504145, No. 11364021, No. 11664014, and No. 11464018 and from the Natural Science Foundation of Jiangxi Province under Grants No. 20161BAB211013, No. 20161BAB201023, and No. 20142BAB212004.

[1] R. Benzi, A. Sutera, and A. Vulpiani, J. Phys. A **14**, L453 (1981).
[2] R. Benzi, G. Parisi, A. Sutera, and A. Vulpiani, Tellus **34**, 10 (1982).
[3] L. Gammaitoni, P. Hänggi, P. Jung, and F. Marchesoni, Rev. Mod. Phys. **70**, 223 (1998).
[4] T. Wellens, V. Shatokhin, and A. Buchleitner, Rep. Prog. Phys. **67**, 45 (2004).
[5] B. Kosko and S. Mitaim, Phys. Rev. E **64**, 051110 (2001).
[6] F. Duan, F. Chapeau-Blondeau, and D. Abbott, Phys. Rev. E **84**, 051107 (2011).
[7] P. Jung and P. Hänggi, Phys. Rev. A **44**, 8032 (1991).
[8] R. L. Badzey and P. Mohanty, Nature (London) **437**, 995 (2205).
[9] R. Almog, S. Zaitsev, O. Shtempluck, and E. Buksa, Appl. Phys. Lett. **90**, 013508 (2007).
[10] H. H. Adamyan, S. B. Manvelyan, and G. Yu. Kryuchkyan, Phys. Rev. A **63**, 022102 (2001).
[11] T. Wellens and A. Buchleitner, J. Phys. A **32**, 2895 (1999).
[12] D. Witthaut, J. Phys. B **45**, 225501 (2012).
[13] M. Grifoni and P. Hänggi, Phys. Rev. Lett. **76**, 1611 (1996).

[14] S. F. Huelga and M. B. Plenio, Phys. Rev. Lett. **98**, 170601 (2007).
[15] S. F. Huelga and M. B. Plenio, Phys. Rev. A **62**, 052111 (2000).
[16] B. Fan and M. Xie, Phys. Rev. A **95**, 023808 (2017).
[17] P. Sen, Phys. Rev. E **63**, 040101 (2001).
[18] E. T. Jaynes and F. W. Cummings, Proc. IEEE **51**, 89 (1963).
[19] Bruce W. Shore and P. L. Knight, J. Mod. Opt. **40**, 1195 (1993).
[20] J. Kerckhoff, M. A. Armen, and H. Mabuchi, Opt. Express **19**, 24468 (2011).
[21] J. M. Fink, L. Steffen, P. Studer, Lev S. Bishop, M. Baur, R. Bianchetti, D. Bozyigit, C. Lang, S. Filipp, P. J. Leek, and A. Wallraff, Phys. Rev. Lett. **105**, 163601 (2010).
[22] K. H. Madsen, S. Ates, T. Lund-Hansen, A. Löffler, S. Reitzenstein, A. Forchel, and P. Lodahl, Phys. Rev. Lett. **106**, 233601 (2011).
[23] H. M. Wiseman and G. J. Milburn, *Quantum Measurement and Control* (Cambridge University, Cambridge, England, 2010).
[24] C. M. Savage and H. J. Carmichael, IEEE J. Quantum Electron. **24**, 1495 (1988).
[25] S. H. Strogatz, *Nonlinear Dynamics and Chaos* (Westview, Boulder, CO, 2001).
[26] L. Gammaitoni, F. Marchesoni, and S. Santucci, Phys. Rev. Lett. **74**, 1052 (1995).
[27] H. A. Kramers, Physica **7**, 284 (1940).
[28] C. W. Gardiner, *Handbook of Stochastic Methods*, 2nd ed. (Springer, New York, 2002).
[29] Th. K. Mavrogordatos, G. Tancredi, M. Elliott, M. J. Peterer, A. Patterson, J. Rahamim, P. J. Leek, E. Ginossar, and M. H. Szymanska, Phys. Rev. Lett. **118**, 040402 (2017).